Large influence of incomplete fusion in $^{12}C + ^{159}Tb$ at $E_{lab} \approx 4$–7 MeV/nucleon

Abhishek Yadav,[1,*] Vijay R. Sharma,[1] Pushpendra P. Singh,[2,†] Devendra P. Singh,[1] Manoj K. Sharma,[3] Unnati Gupta,[1] R. Kumar,[4] B. P. Singh,[1,‡] R. Prasad,[1] and R. K. Bhowmik[4,§]

[1]*Department of Physics, A. M. University, Aligarh (U.P.)-202 002, India*

[2]*GSI Helmholtz Centre for Heavy Ion Research GmbH, Planckstrasse 1, D-64291 Darmstadt, Germany*

[3]*Physics Department, S. V. College, Aligarh (U.P.), India*

[4]*NP-Group, Inter University Accelerator Center, New Delhi-110067, India*

(Received 20 June 2011; revised manuscript received 11 August 2011; published 27 March 2012)

Low energy incomplete fusion has been studied in $^{12}C+^{159}Tb$ system at energies $\approx$ 4–7 MeV/nucleon. The excitation functions of individual reaction channels have been measured using off-line γ spectroscopy, and analyzed in the framework of statistical model code PACE4 based on the concept of equilibrated compound nucleus decay. A significant fraction of incomplete fusion has been found in the production of residues involving α particle(s) in the exit channels. For better insights into the onset and strength of incomplete fusion, the incomplete fusion strength function has been deduced as a function of various entrance channel parameters. Large influence of incomplete fusion has been observed at slightly above barrier energies, and increases smoothly with incident projectile energy. Present results have been compared with the results obtained in the interactions of ^{12}C with nearby targets to probe the dependence of incomplete fusion on entrance channel mass asymmetry. It has been found that the percentage fraction of incomplete fusion increases linearly with mass asymmetry of interacting partners in the studied mass region.

DOI: 10.1103/PhysRevC.85.034614 PACS number(s): 25.60.Dz, 25.70.Gh, 25.70.Jj

I. INTRODUCTION

Considerable efforts are being employed to synthesize superheavy elements using heavy-ion induced complete fusion (CF) reactions [1–6]. In addition to the fission and quasifission [7–12], the existence of incomplete fusion (ICF) [13–27] at low incident energies (i.e., $\approx$ 4–7 MeV/nucleon) may add complexity to the synthesis of superheavy elements. In general, at these energies, CF is supposed to be the sole contributor to the total fusion cross section [26,27]. However, a large fraction of ICF has been observed at energies as low as $\approx$ 4–7 MeV/nucleon [13–21]. The onset of ICF at slightly above barrier energies triggered the resurgent interest to study ICF at these energies. In a qualitative way, CF and ICF processes can be disentangled on the basis of driving angular momenta (ℓ waves) [27–29]. The central and/or near-central interactions ($0 \leqslant \ell \leqslant \ell_{crit}$) form a completely fused composite (CFC) system after intimate contact and transient amalgamation of entire projectile and target nucleus. Eventually, the projectile's kinetic energy and angular momenta are distributed among all the accessible internal degrees of freedom of the composite system, leading to the formation of a fully equilibrated compound nucleus (CN). However, at relatively higher ℓ values ($\geqslant \ell_{crit}$) imparted into the system due to noncentral interactions (or at sufficiently higher energies), the pocket in the entrance channel potential vanishes [28]. As a consequence, fusion of entire projectile is hindered and gives way to ICF. In this case, a part of projectile is emitted as a spectator (P^s) to release excess driving angular momenta. After such an emission, the remnant (participant: P^p) is supposed to carry input angular momenta less than or equal to its own critical limit ($\ell_{eff} \leqslant \ell_{crit}^{P^p+T}$) for fusion to occur [29]. The partial fusion of incident projectile results in an incompletely fused composite (IFC) system, and direct projectile-like fragments (PLFs) are dominantly ejected in the forward cone. The CN formed via CF is expected to have predetermined mass/charge, excitation energy and angular momenta. However, the IFC system is formed with relatively less mass/charge and excitation energy (due to fractional fusion of projectile), but at high angular momenta (imparted into the system in noncentral interactions) as compared to the CN originated from CF process [17].

The concept of partial fusion of projectile in heavy-ion interactions was set in after first experimental observation of 'direct PLFs' emitted in massive transfer reactions by Britt and Quinton [30]. Since then, several experimental/theoretical studies have been carried out to understand ICF dynamics. Some of the important studies are summarized in an outstanding review by Gerschel [31]. However, some of the widely used descriptions of ICF are discussed here for ready reference. Wilczynski *et al.* [29], established ICF as a natural extension of CF for higher ℓ values (above ℓ_{crit}) associated with noncentral interactions. The noncentral nature of ICF has also been emphasized by Geoffroy *et al.* [32], Trautmann *et al.* [33], and Inamura *et al.* [34]. In the breakup fusion (BUF) model [35] of Udagawa and Tamura, the projectile is assumed to break up into constituent α clusters (e.g., $^{12}C \rightarrow {}^{8}Be + \alpha$) within the nuclear field of the target nucleus. The concept of the BUF model modifies the picture of fusion of two nuclei as (i) sequential CF where all projectile fragments fuse with target nucleus, and (ii) ICF where only a part of projectile fuses with target nucleus and the remnant behaves like a spectator.

*abhishekyadav117@gmail.com

†Also at:Institute for Nuclear Physics, TU Darmstadt, Schlossgartenstrasse 9, D-64289 Darmstadt, Germany.

‡bpsinghamu@gmail.com

§Present address:Department of Pure and Applied Physics, Guru Ghasidas University, Koni, Bilaspur - 495009 (CG), India.

The sequential CF is experimentally indistinguishable from direct CF. The total fusion cross section may be defined as the sum of CF and ICF cross sections, i.e., $\sigma_{TF} = \Sigma\sigma_{CF} + \Sigma\sigma_{ICF}$ [26–28]. Further, Morgenstern *et al.* [36] correlated the probability of ICF with the entrance channel mass asymmetry. In Ref. [36], the probability of ICF is found to be higher for more mass-asymmetric systems. It may be pointed out that the existing models/theories fairly explain ICF data obtained at energies $\approx$ 7–10 MeV/nucleon up to some extend, but do not provide satisfactory reproduction of ICF data at lower incident energies. Due to the unavailability of reliable theoretical model to predict low energy ICF, the experimental study of ICF is still an active area of investigations.

The most debated and outstanding issues related to low energy ICF have been, (i) the localization of the ℓ window, (ii) the usefulness of ICF to populate high-spin states in final reaction products, and (iii) the effect of entrance channel parameters on the onset and strength of ICF. In recent years, high quality data on excitation functions (EFs) [18,19,21,23], spin distributions (SDs) [17], and linear momentum distributions [20,22,24] of individual reaction products have been obtained at the Inter-University Accelerator Center (IUAC), New Delhi in a variety of experiments. These studies conclusively demonstrate the low energy ICF but limited only for a few projectile-target combinations. The EFs of individual reaction channels populated in ^{12}C+^{159}Tb system at energies $\approx$ 4–7 MeV/nucleon are presented in this work. Owing to the α-like structure of the projectile, the ICF reaction mechanism is expected to influence the decay channels involving α particles. The ICF strength function has been deduced from the analysis of experimental EFs in the framework of statistical model code PACE4 based on equilibrated compound nucleus decay. In order to generate some systematics, the values of percentage ICF fraction obtained for nearby systems, i.e., ^{12}C+^{103}Rh [37], ^{12}C+^{115}In [38], ^{12}C+^{128}Te [39], ^{12}C+^{159}Tb (this work), ^{12}C+^{165}Ho [40], and ^{12}C+^{169}Tm [41,42], have been compared. This paper is organized as follows. The experimental details and data reduction procedure are discussed in Sec. II. The results obtained in the present work are discussed in connection with the existing data in Sec. III. The outcome of the present work is summarized in the last section of this paper.

II. EXPERIMENTAL DETAILS AND DATA REDUCTION PROCEDURE

The experiment has been performed at the Inter University Accelerator Center (IUAC), New Delhi, India, using off-line γ-ray spectroscopy. Natural ^{159}Tb targets ($t_m \approx$ 1.2–2.5 mg/cm^2) and Al-catcher foils ($t_m \approx$ 1.5–2.5 mg/cm^2) were prepared by rolling technique. An Al-catcher foil of sufficient thickness has been placed behind the target foil so that the recoiling products during the irradiations may be trapped in the catcher foil thickness. To cover a wide energy range in an irradiation, an energy degradation technique has been used. In this experiment, five stacks (each made by three target-catcher foil assemblies) were prepared. The irradiations have been carried out in the general purpose scattering chamber (GPSC) at energies $\approx$ 59, 70, 73, 85, and 88 MeV. An in-vacuum transfer facility has been used to minimize the lapse time between the stop of the irradiation and beginning of the counting of the activity induced in a target-catcher assembly. The incident beam energy on each target foil in a stack has been estimated using the code SRIM [43]. For an example, at the highest incident energy (i.e., $\approx$88 MeV), the uncertainty in the energy is estimated to be $\approx \pm$0.69 MeV, and, at the lowest incident energy (i.e., $\approx$ 54.83) is estimated to be $\approx \pm$0.52 MeV. Considering the half-lives of interest, the irradiations have been carried out for $\approx$ 8–10 h duration for each stack. A Faraday cup has been installed behind the target-catcher foil assembly to measure the beam current. The beam current has been maintain $\approx$25–30 nA during all the irradiations.

The radio activity produced in the target-catcher foil assemblies have been followed by a precalibrated high resolution HPGe detector coupled to a CAMAC based data acquisition system CANDLE [44]. The HPGe detector used in this experiment has been calibrated using standard γ sources, e.g., ^{60}Co, ^{133}Ba, and ^{152}Eu. The efficiency of the detector has been determined using same sources at various source (target-catcher foil assembly)—detector separations to wash out the solid angle effect. The energy resolution of the detector has been estimated $\approx$2.5 keV for 1408 keV γ line of ^{152}Eu source. A 50 Hz pulser was used to determine the dead time of the detector. The source (target-catcher foil assembly)—detector separation has been adjusted to keep the dead-time below 10% during the counting. Reaction residues have been identified by their characteristic γ lines, and confirmed by the decay-curve analysis. As a representative case, a typical γ-ray spectrum obtained at incident energy $\approx$87.31$\pm$0.69 MeV is shown in Fig. 1, and some of the γ peaks corresponding to different CF and/or ICF residues are labeled. The reaction residues expected to be populated via CF and/or ICF in ^{12}C+^{159}Tb system are given in Table I with their spectroscopic properties taken from Refs. [45,46]. The production cross section of the reaction residues (σ_{ER}) have been determined using the standard formulation as given in Ref. [21]. Experimentally measured production cross sections σ_{ER} (mb) of individual reaction residues are given in Tables II and III. It may be pointed out that the errors in the measured production cross sections may arise due to (i) the nonuniformity of target foils, (ii) fluctuations in the beam current during the irradiations, (iii) the uncertainty in geometry dependent efficiency of HPGe detector, and (iv) due to the dead time of the spectrometer. Detailed discussion on the error analysis is given elsewhere [21]. In the present work, the overall error including statistical errors is estimated to be $\leqslant$ 15%, excluding the uncertainty in branching ratio, decay constant, etc., which have been taken from the Table of Radioactive Isotopes [45].

III. OBTAINED RESULTS, ANALYSIS AND THEIR INTERPRETATION

The EFs of ^{168}Lu$^{g+m}(3n)$, ^{167}Lu$(4n)$, ^{165}Lu$(6n)$, ^{167}Yb$(p3n)$, ^{165}Tm$(\alpha 2n)$, ^{163}Tm$(\alpha 4n)$, ^{161}Ho$(2\alpha 2n)$, and ^{160}Ho$(2\alpha 3n)$ radionuclides expected to be populated via CF and/or ICF of ^{12}C with ^{159}Tb have been measured at energies $\approx$ 4–7 MeV/nucleon. In order to understand up to what extent

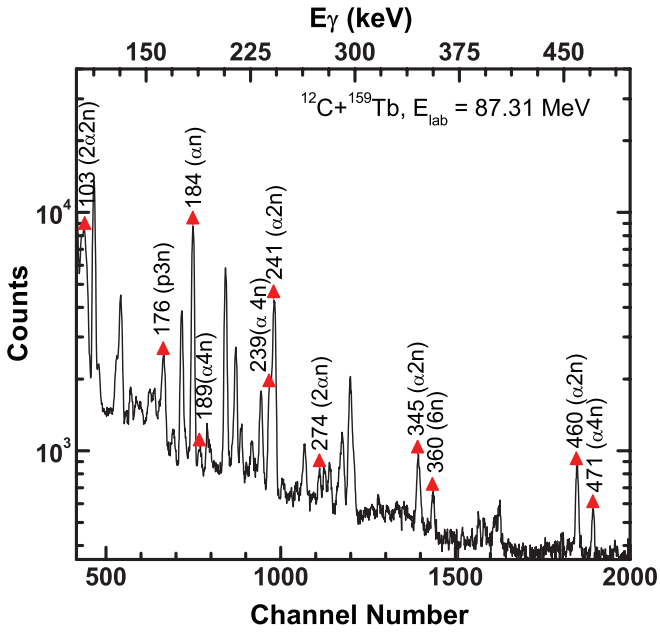

FIG. 1. (Color online) Typical γ-ray spectrum obtained at 87.31±0.69 MeV in ^{12}C+^{159}Tb interactions. Some of the identified γ lines corresponding to different CF and/or ICF residues are labeled.

the decay of these radionuclides can be justified by equilibrated CN decay, experimentally measured EFs are analyzed within the framework of the statistical model code PACE4 [48]. The code PACE4 is based on the Hauser-Feshbach theory of CN decay, and uses statistical approach of CN de-excitation by Monte Carlo procedure. In this code, the angular momentum projections are calculated at each stage of de-excitation, which enables the determination of angular distribution of the emitted particles and angular momentum conservation is explicitly taken into account. The BASS models were used to calculate CF cross sections [47]. The default optical model parameters for neutrons, protons, and α particles are used [48]. The γ-ray strength functions for $E1$, $E2$, and $M1$ transition were taken from tables of Endt [49]. In this code, the level density parameter ($a = A/K$ MeV^{-1}, where A is the mass number of the nucleus and K is a free parameter) is one of the important parameters. The value of free parameter K can be varied to reproduce experimental EFs with in the physically justified limits. It may be pointed out that any enhancement in the EFs predicted by PACE4 may be attributed to some physical effect which is not included in this code.

A. *xn* and *pxn* channels

Figure 2(a) shows the experimentally measured EFs of ^{168}Lu^{g+m}($t_{1/2}$ = 6.7 min, 5.5 min), ^{167}Lu($t_{1/2}$ = 51.5 min), ^{165}Lu($t_{1/2}$= 10.74 min), and ^{167}Yb($t_{1/2}$ = 17.5 min) evaporation residues expected to be populated via $3n$, $4n$, $6n$, and $p3n$ emission from the excited ^{171}Lu* nucleus formed in CF reactions. Self-explanatory notations are used to explain the decay channels in this figure. The solid lines through the data points are drawn to guide the eyes. During the decay-curve analysis, the evaporation residue ^{167}Yb($p3n$) is found to be

TABLE I. List of identified reaction residues (channels) with their spectroscopic properties.

Residue	$T_{1/2}$	J^{π}	E_{γ}(keV)	I^{γ} (%)
^{168}Lu^{g}($3n$)	5.5 min	3^+	198.86	180.0[a]
			228.58	70.0[a]
^{168}Lu^{m}($3n$)	6.7 min	6^-	198.86	180.0[a]
			228.58	70.0[a]
^{167}Lu($4n$)	51.5 min	$7/2^+$	213.21	3.5
^{165}Lu($6n$)	10.74 min	$1/2^+$	120.58	25
			360.51	8.2
^{167}Yb($p3n$)	17.5 min	$5/2^-$	176.2	20.4
			177.26	2.7
^{165}Tm($\alpha 2n$)	30.06 h	$1/2^+$	242.85	35
			346.75	3.9
			356.44	3.7
			460.12	3.7
^{163}Tm($\alpha 4n$)	1.81 h	$1/2^+$	190.07	1.28
			239.67	4.1
			471.29	3.8
^{161}Ho($2\alpha 2n$)	2.48 h	$7/2^-$	103.03	3.6
^{160}Ho^{g}($2\alpha 3n$)	25.6 min	5^+	645.25	16.20
^{160}Ho^{m}($2\alpha 3n$)	5.02 h	2^-	645.25	16.20
			728.18	30.8
			879.39	20.2

[a]These intensities are relative.

strongly fed from its higher charge isobar (precursor hereafter) ^{167}Lu($4n$) through β^+ emission. The half-life of of precursor (i.e., ^{167}Lu $\rightarrow$ $t_{1/2}^{\rm pre}$ = 51.5 min) is larger than the half-life of the daughter nuclei (i.e., ^{167}Yb $\rightarrow$ $t_{1/2}^{d}$ = 17.5 min). In this case, the independent production cross section ($\sigma_{\rm ind}$) of ^{167}Yb has been deduced using the following successive radioactive decay formulation [50]:

$$N_d(t) = C_{t=0}e^{-\lambda_d t} + \frac{(P_{\rm pre}\lambda_{\rm pre})}{(\lambda_d - \lambda_{\rm pre})}N_{\rm pre}(t)e^{-\lambda_{\rm pre}t}, \qquad (1)$$

where $N_d(t)$ and $N_{\rm pre}(t)$ are the number of daughter and precursor nuclei produced at time t. $C_{t=0}$ is the cumulative (precursor + daughter) number of nuclei produced at the end of the irradiation, $\sigma_{\rm pre}$ and σ_d are the production cross sections of precursor and daughter nuclei; and $\lambda_{\rm pre}$ and λ_d are the decay constants of precursor and daughter nuclei, respectively. The value of $N_{\rm pre}(t)$ has been deduced from the experimentally measured decay curve of ^{167}Lu. The value of $N_d(t)$ (^{167}Yb) has been obtained by solving Eq. (1), which has been translated to its production cross section ($\sigma_{\rm ind}$), and is plotted in Fig. 2(a) as independent production of ^{167}Yb$^{\rm (ind)}$($p3n$).

To reproduce the experimental EFs of xn/pxn channels using statistical model code PACE4, and to identify right level density parameter for the analysis of α-emitting channels, different values of the level density parameter have been tested by varying the free parameter K (i.e, K = 8–12). Values of the level density parameter K significantly higher than $K = 8$ are expected to not be appropriate for the excitation energies involved in the studied reactions. Nevertheless, we have considered them in the calculations to better enlighten the dependence of the calculated excitation functions on this

TABLE II. Experimentally measured production cross sections σ(mb) of $^{168}Lu^{g+m}$, ^{167}Lu, ^{165}Lu, ^{167}Yb, ^{165}Tm, and ^{163}Tm residues.

E_{lab} (MeV)	$^{168}Lu^{g+m}$(CF)	^{167}Lu(CF)	^{165}Lu(CF)	^{167}Yb(CF)	^{165}Tm (CF+ICF)	^{163}Tm (CF+ICF)
54.83 + 0.52	184.5 ± 29.68	12.12 ± 2	–	0.2 ± 0.03	–	–
58.51 + 0.50	177.5 ± 24.2	155.23 ± 23.25	–	1 ± 0.13	13.66 ± 1.9	
61.37 + 0.63	118 ± 15.27	340.15 ± 51	–	10 ± 1.9	16.65 ± 2.5	–
62.63 + 0.80	94.5 ± 12.85	545.2 ± 79	–	15 ± 2.19	19.61 ± 2.65	1 ± 0.09
65.49 + 0.69	47.5 ± 6.95	635.2 ± 93.45	–	19.5 ± 2.45	17.45 ± 2.13	8 ± 1.09
67.24 + 1.17	45 ± 6.25	649.3 ± 85	–	49 ± 6.5	12.52 ± 1.56	22.0 ± 2.6
69.15 + 0.85	14 ± 3.01	699.5 ± 102.9	–	55.34 ± 7.9	10.16 ± 1.3	58.41 ± 7.98
72.24 + 0.76	7.5 ± 1.26	499.6 ± 70.68	0.03 ± 0.005	45.8 ± 6.62	8.76 ± 1.5	108.17 ± 15.63
74.97 + 0.57	2.5 ± 0.29	298.4 ± 42.1	2 ± 0.3	19.2 ± 2.59	8.21 ± 0.96	129.68 ± 18.5
77.77 + 0.62	1 ± 0.15	149.6 ± 19.5	36 ± 4.5	29 ± 4.2	8.98 ± 1.12	202.54 ± 32
79.62 + 0.61	0.5 ± 0.08	150 ± 19.8	58 ± 8.5	11 ± 1.5	9.98 ± 1.38	189.90 ± 28.65
82.47 + 0.82	0.15 ± 0.03	89.9 ± 12.65	301 ± 46	8 ± 1.02	12.04 ± 1.56	211.26 ± 26.65
84.44 + 0.56	0.1 ± 0.02	35.3 ± 4.5	408 ± 58.9	4.5 ± 0.5	17.79 ± 2.67	204.10 ± 29.4
87.31 + 0.69	0.01 ± 0.0015	23.2 ± 3.9	745 ± 109.5	4 ± 0.45	18.9 ± 2.34	212.23 ± 25.69

parameter. Figure 2(b) shows the experimental EFs of all xn/pxn channels (i.e., $\Sigma\sigma_{CF}^{exp}$) compared with PACE4 predictions. As shown in this figure, the value of $\Sigma\sigma_{CF}^{exp}$ is very well reproduced by PACE4 for the level density parameter $a = A/8$ MeV^{-1}. This indicates the production of these residues through the de-excitation of fully equilibrated compound nucleus decay formed in a CF reaction.

B. α-emitting channels

The experimental EFs of $^{165}Tm(\alpha 2n)$, $^{163}Tm(\alpha 4n)$, $^{161}Ho(2\alpha 2n)$, and $^{160}Ho^{g+m}(2\alpha 3n)$ residues are shown in Fig. 3(a)–3(d). Due to the involvement of α emission in the exit channel, these residues are expected to be populated via both CF and/or ICF processes. It has been found during the decay-curve analysis that the evaporation residue ^{165}Tm is strongly fed from its precursor ^{165}Yb. In this case, the half-life of the precursor (i.e., $^{165}Yb \rightarrow t_{1/2}^{pre} = 9.9$ min) is smaller than the daughter nuclei (i.e.,$^{165}Tm \rightarrow t_{1/2}^{d} = 30.06$ h). As demonstrated by Cavinato *et al.* [50], the independent production cross section (σ_{ind}) of daughter nuclei may be defined in terms of cumulative (σ_{cum}) and precursor (σ_{pre}) cross sections as follows:

$$\sigma_{ind} = \sigma_{cum} - F_{pre}\sigma_{pre}. \quad (2)$$

Here F_{pre} is the precursor coefficient which depends on the branching ratio of precursor decay (P_{pre}) to the final nucleus as

$$F_{pre} = P_{pre}\frac{t_{1/2}^{d}}{\left(t_{1/2}^{d} - t_{1/2}^{pre}\right)}. \quad (3)$$

Here $t_{1/2}^{pre}$ and $t_{1/2}^{d}$ are the half-lives of the precursor and final nuclei, respectively. The values of half-lives and branching ratio of precursor decay (P_{pre}) have been taken from Refs. [45,46]. After the inclusion of these observables, the

TABLE III. Experimentally measured production cross sections σ (mb) of ^{161}Ho and $^{160}Ho^{g+m}$ residues along with the $\Sigma\sigma_{CF}$, $\Sigma\sigma_{ICF}$, σ_{TF} and F_{ICF} (%).

E_{lab} (MeV)	^{161}Ho (CF+ICF)	$^{160}Ho^{g}$ (CF+ICF)	$^{160}Ho^{m}$ (CF+ICF)	$\Sigma\sigma_{CF}$	$\Sigma\sigma_{ICF}$	σ_{TF}	F_{ICF}(%)
54.83 + 0.52	–	–	–	173	–	173	–
58.51 + 0.50	–	–	–	385	6.02	394.06	1.54
61.37 + 0.63	–	–	–	529	12.40	539.96	2.29
62.63 + 0.80	–	–	–	588	16.78	602.97	2.78
65.49 + 0.69	–	–	–	710	30.79	731.08	4.16
67.24 + 1.17	–	–	–	779	42.91	808.68	5.22
69.15 + 0.85	1.37 + 0.18	–	–	849	59.12	913.39	6.51
72.24 + 0.76	4.49 + 0.56	–	–	953	92.02	1066.37	8.81
74.97 + 0.57	6.25 + 1.10	2.37 + 0.29	1.41 + 0.21	1040	122.29	1170.42	10.52
77.77 + 0.62	7.50 + 0.95	5.42 + 0.75	1.55 + 0.23	1110	162.06	1304.84	12.42
79.62 + 0.61	6.34 + 0.89	5.71 + 0.84	1.83 + 0.25	1160	173.64	1336.42	12.99
82.47 + 0.82	5.31 + 0.75	6.45 + 0.91	2.24 + 0.36	1230	185.65	1419.18	13.08
84.44 + 0.56	4.50 + 0.65	7.89 + 1.25	2.56 + 0.34	1270	199.83	1453.13	13.75
87.31 + 0.69	2.10 + 0.32	6.09 + 0.86	2.00 + 0.31	1320	207.8	1501.73	13.84

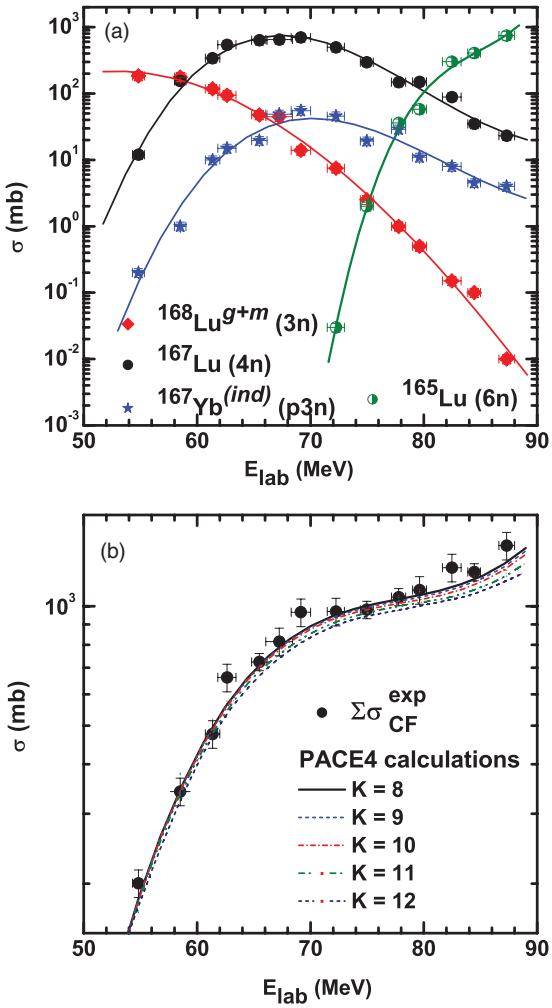

FIG. 2. (Color online) (a) Experimental EFs of ^{168}Lu$^{g+m}(3n)$, ^{167}Lu$(4n)$, ^{165}Lu$(6n)$, and ^{167}Yb$(p3n)$ residues populated in the ^{12}C+^{159}Tb system. The solid lines through the data points are drawn to guide the eyes. (b) Sum of experimentally measured EFs of all xn/pxn channels ($\Sigma\sigma^{\rm exp}_{\rm CF}$) are compared with that predicted by PACE4 for different values of level density parameter ($a = A/K$ MeV^{-1}, where $K = 8$–12).

independent production cross section ($\sigma_{\rm ind}$) can be written as

$$\sigma_{\rm ind} = \sigma_{\rm cum} - P_{\rm pre}\frac{t^d_{1/2}}{\left(t^d_{1/2} - t^{\rm pre}_{1/2}\right)}\sigma_{\rm pre}. \quad (4)$$

As has already been mentioned, the production of ^{165}Tm$(\alpha 2n)$ is substantially fed (with a branching ratio $P_{\rm pre} = 1$) from its precursor ^{165}Yb. The value of $F_{\rm pre}$ is found to be 1.0055 ± 0.001 for the given combination of precursor and final nuclei, providing

$$\sigma_{\rm ind}(^{165}{\rm Tm}) = \sigma_{\rm cum} - 1.0055.\sigma_{\rm pre}. \quad (5)$$

The value of $\sigma_{\rm ind}$ of ^{165}Tm$(\alpha 2n)$ as given above is plotted in Fig. 3(a).

It may be pointed out that the residues populated via α-emitting channels may arise from both CF and/or ICF processes. In the case of CF, the incident projectile (^{12}C) entirely fuses with target nucleus (^{159}Tb) to form a fully equilibrated CN, which may eventually decay via an αxn channel. However, in the case of ICF, only a part of incident projectile (i.e., $^{12}{\rm C} \rightarrow {}^{8}{\rm Be} + \alpha$) fuses with the target nucleus to form an incompletely fused composite system, and the remnant α or ^{8}Be goes on moving in the forward cone as a spectator.

The fraction of ICF in α-emitting channels can be accounted by analyzing EFs of evaporation residues in the framework of statistical model code PACE4 . As mentioned in the previous section, the code PACE4 does not take ICF into account, therefore, any enhancement in the experimental EFs over the PACE4 predictions may be attributed to contribution coming from ICF. The experimental EFs of individual α-emitting channels (expected to be populated via both CF and/or ICF processes) are compared with PACE4 predictions in Fig. 3(a)–3(d). The PACE4 calculations has been performed using same set of input parameters which has been used to reproduce xn/pxn channels. Solid black curves are the best fit to the PACE4 predictions for level density parameter $a = A/8$ MeV^{-1}. As can be seen in Fig. 3(a)–3(d), in general, PACE4 underpredicts the experimental EFs of these residues. The experimentally observed higher production cross section over PACE4 predictions may be attributed to the ICF processes, its contribution being distributed over the full range of energy of the EFs, with a different behavior depending on the residue. Particularly interesting is the trend of the EF measured for ^{165}Tm, which appears to reflect the interplay between CF and ICF processes through three different decay channels:

(i) CF-1: the CF of ^{12}C with ^{159}Tb leads to an excited nucleus ^{171}Lu* which may decay via two protons and four neutrons ($2p4n$ channel) as

$$^{12}{\rm C} + {}^{159}{\rm Tb} \Rightarrow {}^{171}{\rm Lu}^* \Rightarrow {}^{165}{\rm Tm} + 2p4n,$$
$$Q\ \text{value} = -53.47\ \text{MeV},$$
$$E_{\rm thr.} = 57.50\ \text{MeV}.$$

(ii) CF-2: the excited ^{171}Lu* nucleus formed in a CF reaction may decay through an α cluster and two neutrons ($\alpha 2n$ channel) as

$$^{12}{\rm C} + {}^{159}{\rm Tb} \Rightarrow {}^{171}{\rm Lu}^* \Rightarrow {}^{165}{\rm Tm} + \alpha 2n,$$
$$Q\ \text{value} = -25.17\ \text{MeV},$$
$$E_{\rm thr.} = 27.07\ \text{MeV}.$$

(iii) ICF: only a part of projectile ^{12}C (i.e., ^{8}Be) fuses with ^{159}Tb to form an incompletely fused composite system (^{167}Tm*) while an α cluster flows in the forward direction as a spectator. The excited ^{167}Tm* may then decay via two neutrons ($2n$) as

$$^{12}{\rm C}(^{8}{\rm Be} + \alpha) \Rightarrow {}^{8}{\rm Be} + {}^{159}{\rm Tb} \Rightarrow {}^{167}{\rm Tm}^*$$
$$\Rightarrow {}^{165}{\rm Tm} + \alpha + 2n,$$
$$(\text{`}\alpha\ \text{particle'}\ \text{as a spectator}),$$
$$Q\ \text{value} = -17.80\ \text{MeV},$$
$$E_{\rm thr.} = 18.70\ \text{MeV}.$$

The contributions expected from different decay paths as discussed above are marked by red dash dotted (CF1+CF2+ICF) and blue (mainly ICF) dotted lines drawn through the experimental data points in Fig. 3(a). As shown in

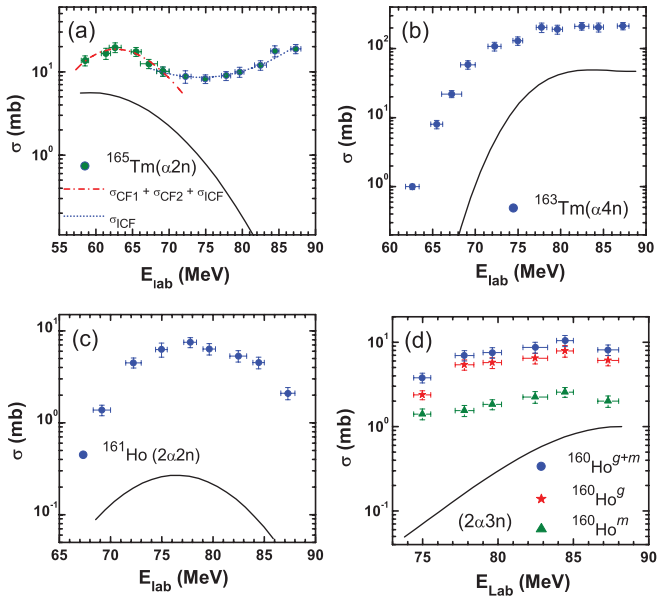

FIG. 3. (Color online) Experimentally measured EFs of evaporation residues ^{165}Tm($\alpha 2n$), ^{163}Tm($\alpha 4n$), ^{161}Ho($2\alpha 2n$), and ^{160}Ho^{g+m}($2\alpha 3n$) are compared with the PACE4 predictions. Solid black curves represent PACE4 predictions performed for $a = A/8$ MeV^{-1}. In (a), red dash dotted and blue dotted lines through the data points are drawn to explain the trend of excitation function. See text for explanation.

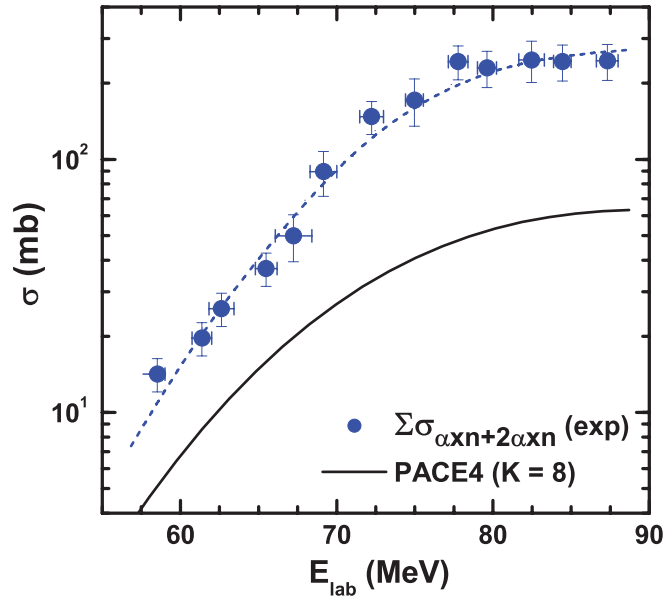

FIG. 4. (Color online) Experimentally measured and theoretically predicted EFs of all α-emitting channels are compared. Physically justified level density parameter $a = A/8$ MeV^{-1} is used in PACE4 calculations. The value of $(\Sigma\sigma^{\rm exp}_{\alpha xn+2\alpha xn})$ is significantly higher than that predicted by PACE4, which may be attributed to the contribution of ICF. Lines through the data points are drawn to guide the eyes.

this figure, the contributions coming from the type CF1 and CF2 (i.e., the contributions of $2p4n$ and/or $\alpha 2n$) are peaking at ≈63 MeV. However, for the energies above ≈70 MeV, PACE4 predicts very low cross-section as compared to the experimental data points. As such, it can be inferred that the ICF significantly contributes to the production of ^{165}Tm residue through α(as a spectator)+$2n$ channel.

Further, for better visualization of ICF fraction in α-emitting channels, the sum of all identified α-emitting channels $(\Sigma\sigma^{\rm exp}_{\alpha xn+2\alpha xn})$ is compared with that estimated by statistical model code PACE4 $(\Sigma\sigma^{\rm PACE4}_{\alpha xn+2\alpha xn})$ in Fig. 4. As shown in this figure, the experimentally measured EFs of $\alpha xn/2\alpha xn$ channels are significantly higher than PACE4 predictions for the same value of level density parameter (i.e., $a = A/8$ MeV^{-1}), which has been used to reproduce CF residues in the present work. Since, the statistical model code PACE4 does not take ICF into account, therefore, the observed enhancement in the experimentally measured EFs over the theoretically predicted ones, points toward the contribution of ICF in the production of these residues.

In order to deduce ICF contribution in $\alpha xn/2\alpha xn$ channels, the same data reduction procedure has been used as given in Refs. [15,19,21]. The contribution of ICF in the production of ^{165}Tm, ^{163}Tm, ^{161}Ho, and ^{160}Ho^{g+m} residues has been accounted as $\Sigma\sigma_{\rm ICF} = \Sigma\sigma_{\rm exp} - \Sigma\sigma_{\rm PACE4}$. In recent reports [20,22,24], the fraction of ICF deduced using above data reduction procedure has been found to be in good agreement with that estimated from the analysis of forward ranges and angular distributions of heavy recoils. In order to see how does ICF contributes to the total reaction cross section ($\sigma_{\rm TF} = \Sigma\sigma_{\rm CF} + \Sigma\sigma_{\rm ICF}$), systematically deduced ICF cross section ($\Sigma\sigma_{\rm ICF}$) is plotted with the sum of all CF channels ($\Sigma\sigma_{\rm CF}$) and $\sigma_{\rm TF}$ as a function of incident projectile energy in Fig. 5. For better visualization of increasing ICF contribution with energy, the value of $\Sigma\sigma_{\rm ICF}$ is plotted in the inset. As shown in this figure, the increasing separation between $\Sigma\sigma_{\rm CF}$ and $\sigma_{\rm TF}$ with incident projectile energy indicates energy dependence of ICF.

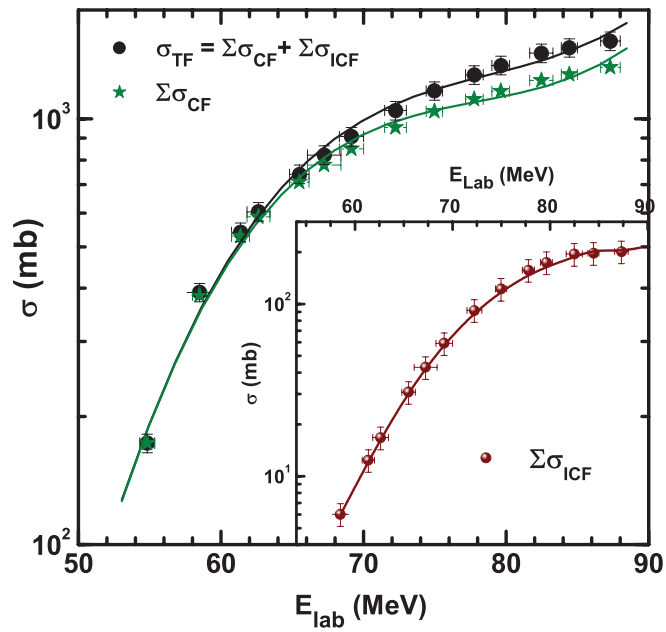

FIG. 5. (Color online) The total fusion cross section ($\sigma_{\rm TF}$), the sum of all CF ($\Sigma\sigma_{\rm CF}$), and ICF ($\Sigma\sigma_{\rm ICF}$) channels are plotted as a function of incident projectile energy. Lines through the data points are drawn to guide the eyes.

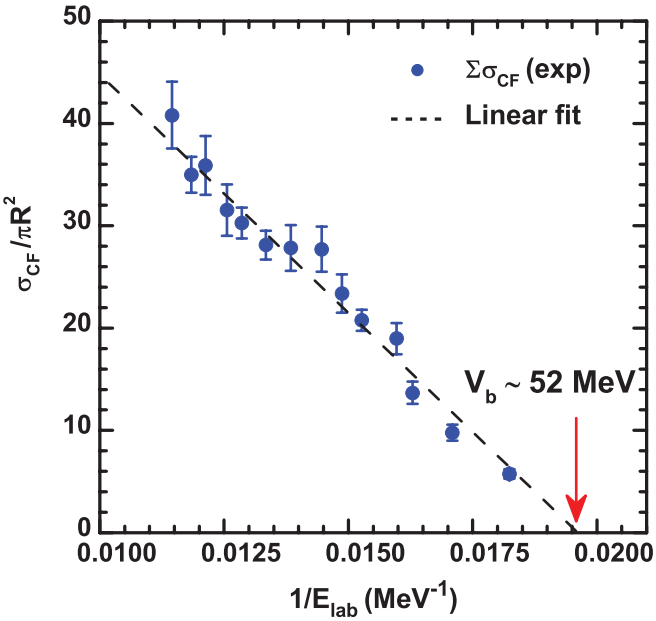

FIG. 6. (Color online) The reproduction of Coulomb barrier (V_b) of ^{12}C+^{159}Tb system from the analysis of the experimentally measured CF cross sections. The dashed line through the data points is achieved by best fitting procedure of data.

To support our measurement and the adopted data reduction procedure, an attempt has been made to deduce the value of fusion barrier (V_b) from the analysis of experimentally measured CF excitation functions. According to Gutbrod *et al.* [51], the CF probability may be given as

$$\Sigma\sigma_{\rm CF} = \pi R^2(1 - V_b/E_{\rm lab}). \quad (6)$$

If the normalized value of $\Sigma\sigma_{\rm CF}$ is plotted as a function of $1/E_{\rm lab}$, it should show a linear decrease. The normalized value of $\Sigma\sigma_{\rm CF}$ has been plotted as a function of $1/E_{\rm lab}$ in Fig. 6. As shown in this figure, the data points can be fitted by a linear equation which intersects the x axis at $E_{\rm lab}$ corresponding to ≈52 MeV. This confirms the value of fusion barrier ($V_b \approx 52$ MeV) of ^{12}C+^{159}Tb system, and strengthen the present measurements and the data reduction procedure. Further, the percentage fraction of ICF ($F_{\rm ICF}$) has been deduced as a function of various entrance channel parameters, and is discussed in the following sections.

C. ICF strength function

For better insights into the onset and influence of ICF, the percentage fraction of incomplete fusion ($F_{\rm ICF}$) has been deduced from the analysis of data as demonstrated in Ref. [19]. The $F_{\rm ICF}$ is a measure of relative strength of ICF to the total fusion, and defined as $F_{\rm ICF}(\%) = (\Sigma\sigma_{\rm ICF}/\sigma_{\rm TF})\times 100$. The value of $F_{\rm ICF}$ is plotted as a function of reduced incident projectile energy ($E_{\rm lab}/V_b$) in Fig. 7, i.e., termed as ICF strength function. The ICF strength function defines empirical probability of ICF at different incident projectile energies. As shown in this figure, the value of $F_{\rm ICF}$ is found to be ≈ 1.5% at $1.12V_b$ (i.e., ≈ 12% above the barrier), and increases smoothly

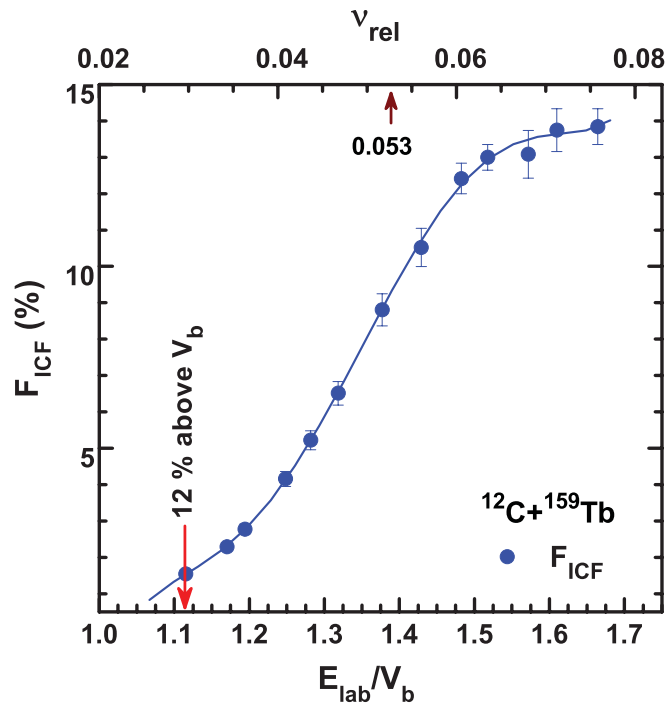

FIG. 7. (Color online) The percentage fraction of ICF ($F_{\rm ICF}$) for ^{12}C+^{159}Tb system as a function of reduced incident projectile energy ($E_{\rm lab}/V_b$). The value of $F_{\rm ICF}$ smoothly increases from ≈1.5% (at $1.12V_b$) to ≈14% (at $1.64V_b$) in the measured energy range. The line is drawn to guide the eyes.

up to ≈ 14% at the highest measured energy (i.e., $1.64V_b$) for ^{12}C+^{159}Tb system. The observed increasing trend of $F_{\rm ICF}$ with energy indicates that the breakup probability of incident projectile increases under the influence of increasing input angular momenta. The incident projectile (^{12}C) may break up into several combinations of α clusters to yield ICF. Some of the breakup combinations observed in previous studies are (i) ^{12}C may break up into ^{8}Be and ^{4}He(α) clusters, and/or (ii) three α fragments [38–40]. Depending on the favorable input angular momentum conditions, one or a group of fragments (in successive mode) may fuse with the target nucleus to form an incompletely fused composite system [17].

Further, it may not be out of place to mention that some of the reaction channels could not be measured due to the shorthalf-lives of these missing channels in the present work, which is the limitations of employed technique. In order to incorporate the missing CF channels, the value of $\Sigma\sigma_{\rm CF}$ has been corrected using PACE4 predictions. However, no correction could made to incorporate missing ICF channels. Therefore, the quoted value of $\Sigma\sigma_{\rm ICF}$ in Fig. 5 should be treated as the lower limit of ICF for this system. The inclusion of missing ICF channels may modify slightly the picture presented in Fig. 7.

D. ICF dependence on entrance channel mass asymmetry

As suggested by Morgenstern *et al.* [36], the ICF contributes significantly above $v_{\rm rel} \approx 0.06$ (6% of c) for more mass-asymmetric systems. In order to test Morgenstern's mass-asymmetry systematics, and to understand how the ICF

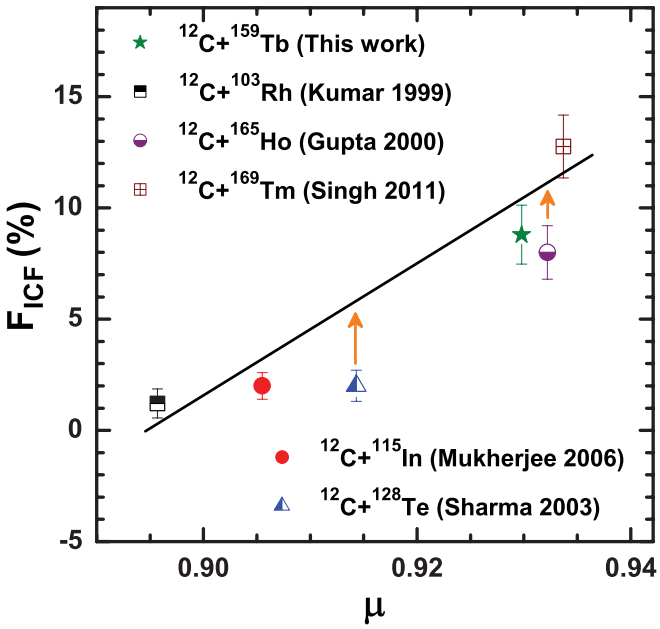

FIG. 8. (Color online) A comparison of the values of $F_{\rm ICF}$ deduced at a constant relative velocity ($v_{\rm rel} = 0.053$) for various systems as a function of entrance channel mass asymmetry (μ). The arrows indicate that the present value of $F_{\rm ICF}$ for ^{12}C+^{128}Te,^{165}Ho systems is expected to go up as discussed in the text.

fraction varies with the entrance channel mass asymmetry ($\mu = A_T/(A_T + A_P)$, the value of $F_{\rm ICF}$ in ^{12}C+^{159}Tb system is compared with that obtained in ^{12}C+^{103}Rh [37], ^{12}C+^{115}In [38], ^{12}C+^{128}Te [39], ^{12}C+^{165}Ho [40], and ^{12}C+^{169}Tm [41,42] systems at a constant relative velocity (i.e., $v_{\rm rel}$ = 0.053). Figure 8 shows the ICF strength ($F_{\rm ICF}$) as a function of μ at $v_{\rm rel} = 0.053$. Solid line through the data points is drawn to guide the eyes. As shown in this figure, the data plotted for six targets agree reasonably well with Morgenstern's mass-asymmetry systematics developed for energies $\geqslant$10 MeV/nucleon. Symbols are used to indicate different target nuclei. As displayed in this figure, the data plotted for six target nuclei for only ^{12}C beam agree reasonably well with Morgenstern's mass-asymmetry systematics. In general, the probability of ICF increases with the entrance channel mass asymmetry. However, the values of $F_{\rm ICF}$ for ^{12}C+^{128}Te and ^{12}C+^{165}Ho systems are slightly away from the increasing trend shown with the straight line. It may be because of the fact that in case of ^{12}C+^{128}Te and ^{12}C+^{165}Ho systems all α-emitting channels could not be measured due to their short half-lives and/or very low γ intensities. The present values of $F_{\rm ICF}$ for ^{12}C+^{128}Te and ^{12}C+^{165}Ho systems are expected to go up if all possible α-emitting channels are measured.

IV. SUMMARY AND CONCLUSIONS

In this work, the EFs of several radionuclides populated via CF and/or ICF in ^{12}C+^{159}Tb system have been measured for the energy range ≈4–7 MeV/nucleon, and analyzed in the framework of equilibrated CN decay using statistical model code PACE4. During the decay curve analysis for the identification of different reaction products, it has been found that some of the *pxn* and *αxn* channels have contribution from precursor decay of higher charge isobar. An attempt has been made to deduce the independent production cross section from cumulative and precursor decay contribution. The experimentally measured EFs of *xn*/*pxn* channels have been found to agree reasonably well with the predictions of statistical model code PACE4, indicating their production via CF only. However, in the case of all α-emitting channels, a significant enhancement in the production cross sections has been observed as compared to the PACE4 predictions. This enhancement has been attributed to the ICF of ^{12}C with ^{159}Tb. It has been observed that the probability of ICF increases with incident projectile energy, and mass asymmetry and/or target mass. The results presented in this work are found to follow Morgenstern's mass-asymmetry systematics [36]. On the basis of results and analysis presented, it may be concluded that apart from CF, the ICF is also a process of greater importance at incident projectile energies ≈ 4–7 MeV/nucleon. The ICF fraction strongly depends on the entrance channel properties, such as mass asymmetry (or the Coulomb factor $Z_P Z_T$), and incident projectile energies. It may, however, be pointed out that the system studied in the present work is rather light, which may not cater to the requirement of synthesizing super heavy elements. However, a rich data set from medium to heavy targets may help to develop some systematics to understand the probability of involved reaction processes at these energies, which may be useful in the super heavy element research. For further refinement of the outcome of this work, the measurement of forward recoil ranges and spin distributions from near barrier energies to well above it are in order.

ACKNOWLEDGMENTS

The authors thank the Inter-University Accelerator Center (IUAC), New Delhi and Department of Physics, AMU, Aligarh for extending necessary facilities to perform this work. We are also thankful to Mr. S. Muralithar and R. P. Singh for scientific discussions and support during the experiments. One of the authors (A.Y.) thanks to the University Grant Commission (UGC) of the Government of India for S.R.F., B.P.S., and R.P. thank the Department of Science and Technology (DST) and the UGC for financial support.

[1] Yu. Ts. Oganessian *et al.*, Nature (London) **400**, 242 (1999), and references therein.
[2] S. Hofmann *et al.*, Eur. Phys. J. A **32**, 251 (2007); **14**, 147 (2002).
[3] K. Siwek-Wilczynska, I. Skwira, and J. Wilczynski, Phys. Rev. C **72**, 034605 (2005).
[4] V. I. Zagrebaev, Nucl. Phys. A **734**, 164 (2004).
[5] Robert Smolanczuk, Phys. Rev. C **59**, 2634 (1999).
[6] Sushil Kumar *et al.*, J. Phys. G: Nucl. Part. Phys. **29**, 625 (2003).
[7] R. du Rietz *et al.*, Phys. Rev. Lett. **106**, 052701 (2011), and references therein.
[8] D. J. Hinde, R. duRietz, M. Dasgupta, R. G. Thomas, and L. R. Gasques, Phys. Rev. Lett. **101**, 092701 (2008), and references therein.

[9] R. G. Thomas *et al*., Phys. Rev. C **77**, 034610 (2008).
[10] I. M. Itkis *et al*., Phys. Rev. C **83**, 064613 (2011).
[11] S. Heinz *et al*., Eur. Phys. J. A **43**, 181 (2010).
[12] K. Nishio *et al*., Phys. Rev. C **77**, 064607 (2008).
[13] A. Diaz-Torres, D. J. Hinde, J. A. Tostevin, M. Dasgupta, and L. R. Gasques, Phys. Rev. C **65**, 024606 (2002); Phys. Rev. Lett. **98**, 152701 (2007).
[14] E. Z. Buthelezi *et al*., Nucl. Phys. A **734**, 553 (2004).
[15] P. R. S. Gomes, I. Padron, E. Crema, O. A. Capurro, J. O. FernandezNiello, A. Arazi, G. V. Marti, J. Lubian, M. Trotta, A. J. Pacheco, J. E. Testoni, M. D. Rodriguez, M. E. Ortega, L. C. Chamon, R. M. Anjos, R. Veiga, M. Dasgupta, D. J. Hinde, and K. Hagino, Phys. Rev. C **73**, 064606 (2006); Phys. Lett. B **601**, 20 (2004).
[16] M. Dasgupta *et al*., Nucl. Phys. A **787**, 144 (2007).
[17] Pushpendra P. Singh *et al*., Phys. Lett. B **671**, 20 (2009); Phys. Rev. C **80**, 064603 (2009); **78**, 017602 (2008).
[18] Pushpendra P. Singh *et al*., J. Phys.: Conf. Ser. **282**, 012019 (2011); Euro. Phys. J. Web of Conferences **2**, 10004 (2010).
[19] Pushpendra P. Singh *et al*., Phys. Rev. C **77**, 014607 (2008), and references therein.
[20] Pushpendra P. Singh *et al*., Eur. Phys. J. A **34**, 29 (2007).
[21] Unnati Gupta *et al*., Nucl. Phys. A **811**, 77 (2008).
[22] Unnati Gupta *et al*., Phys. Rev. C **80**, 024613 (2009).
[23] Devendra P. Singh *et al*., Phys. Rev. C **80**, 014601 (2009).
[24] Devendra P. Singh *et al*., Phys. Rev. C **81**, 054607 (2010).
[25] D. J. Hinde, M. Dasgupta, B. R. Fulton, C. R. Morton, R. J. Wooliscroft, A. C. Berriman, and K. Hagino, Phys. Rev. Lett. **89**, 272701 (2002).
[26] M. Dasgupta, P. R. S. Gomes, D. J. Hinde, S. B. Moraes, R. M. Anjos, A. C. Berriman, R. D. Butt, N. Carlin, J. Lubian, C. R. Morton, J. O Newton, and A. SzantodeToledo, Phys. Rev. C **70**, 024606 (2004).
[27] L. F. Canto, R. Donangelo, L. M. deMatos, M. S. Hussein, and P. Lotti, Phys. Rev. C **58**, 1107 (1998).
[28] P. E. Hodgson, E. Gadioli, and E. Gadioli Erba, *Introductory Nuclear Physics* (Clarendon Press, Oxford, 1997), Chap. 23.
[29] J. Wilczynski *et al*., Phys. Rev. Lett. **45**, 606 (1980); Nucl. Phys. A **373**, 109 (1982).
[30] H. C. Britt and A. R. Quinton, Phys. Rev. **124**, 877 (1961).
[31] C. Gerschel, Nucl. Phys. A **387**, 297 (1982).
[32] K. A. Geoffroy, D. G. Sarantites, M. L. Halbert, D. C. Hensley, R. A. Dayras, and J. H. Barker, Phys. Rev. Lett. **43**, 1303 (1979).
[33] W. Trautmann, O. Hansen, H. Tricoire, W. Hering, R. Ritzka, and W. Trombik, Phys. Rev. Lett. **53**, 1630 (1984).
[34] T. Inamura *et al*., Phys. Lett. B **68**, 51 (1977); **84**, 71 (1982); T. Inamura, A. C. Kahler, D. R. Zolnowski, U. Garg, T. T. Sugihara, and M. Wakai, Phys. Rev. C **32**, 1539 (1985).
[35] T. Udagawa and T. Tamura, Phys. Rev. Lett. **45**, 1311 (1980).
[36] H. Morgenstern, W. Bohne, W. Galster, K. Grabisch, and A. Kyanowski, Phys. Rev. Lett. **52**, 1104 (1984); Z. Phys. A **313**, 39 (1983); Phys. Lett. B **113**, 463 (1982).
[37] B. B. Kumar, A. Sharma, S. Mukherjee, S. Chakrabarty, P. K. Pujari, B. S. Tomar, A. Goswami, S. B. Manohar, and S. K. Datta, Phys. Rev. C **59**, 2923 (1999).
[38] S. Mukherjee *et al*., Int. J. Mod. Phys. E **15**, 237 (2006).
[39] Manoj K. Sharma *et al*., J. Phys. Soc. Jpn. **72**, 1917 (2003).
[40] S. Gupta, B. P. Singh, M. M. Musthafa, H. D. Bhardwaj, and R. Prasad, Phys. Rev. C **61**, 064613 (2000).
[41] S. Chakrabarty *et al*., Nucl. Rhys. A **678**, 355 (2000).
[42] Pushpendra P. Singh *et al*. (to be published in Phys. Lett. B).
[43] The Stopping and Range of Ions in Matter (SRIM) code: [http://www.srim.org/SRIM/SRIMLEGL.htm].
[44] CANDLE-Collection and Analysis of Nuclear Data using Linux nEtwork, B. P. Ajith Kumar *et al*., DAE **SNP**, 2001, Kolkotta.
[45] E. Browne and R. B. Firestone, *Table of Radioactive Isotopes* (Wiley, New York, 1986).
[46] *Table of Isotopes*, 8th ed., edited by R. B. Firestone and V. S. Shirley (Wiley, New York, 1996).
[47] R. Bass, Nucl. Phys. A **231**, 45 (1974).
[48] A. Gavron, Phys. Rev. C **21**, 230 (1980).
[49] P. M. Endt, At. Data Nucl. Data Tables **26**, 47 (1981).
[50] M. Cavinato *et al*., Phys. Rev. C **52**, 2577 (1995).
[51] H. H. Gutbrod *et al*., Phys. Rev. Lett. **30**, 1259 (1973).